

Louise Pellerin*, U.S. Geological Survey; Jeffery M. Johnston, University of Utah Research Institute; Gerald W. Hohmann (deceased), formerly University of Utah

Summary

The interpretation of electromagnetic (EM) data using one-dimensional (1-D) inversion algorithms can be expected to provide poor resolution of two-dimensional (2-D) and three-dimensional (3-D) structures. Unfortunately 2- or 3-D inversion of large datasets is computationally costly both in processing time and computer memory. Therefore we approach multi-dimensional interpretation with an inversion algorithm, based upon a Born approximation to the 3-D integral equation, that iteratively refines a piece-wise 1-D interpretation at a receiver using the data from neighboring receivers. We test the algorithm on the central-loop response of two 3-D models: a simple prism representing the problem of low-contrast resistivity mapping, and a conductive out-flow plume to simulate mapping of a conductive contaminant plume. Discretization of the first test model exactly matches that of the inversion and illustrates the strengths and weakness of the scheme. The second model is discretized such that its response simulates field data. The test results indicate our method does indeed improve a 1-D interpretation and has merit as a tool in multi-dimensional EM interpretation.

Introduction

Newman et al.,(1987), Blohm et al., (1991), and Taylor et al., (1992) showed that 1-D EM inversions do not accurately recover 2-D and 3-D structures. Laterally biased interpretations can be expected when 1-D interpretation is applied to the response of complex structures. Nevertheless, EM data collected in geophysical exploration are typically interpreted using 1-D inversion routines, without regard to the complexity of the local geoelectric environment, because of the computational expense of a full 3-D inversion for a large survey (Eaton, 1989). In an effort to account for the 3-D EM response and still remain computationally practical, we sequentially perform local 3-D inversion to a particular sounding using only its response and those of its nearest neighbors. Our method thus partitions a large survey into a series of small ones. Use of soundings from adjacent stations provides lateral electric field information for the inversion scheme, thereby removing many of the distortions present in 1-D interpretation.

The algorithm employs a Born approximation to a 3-D integral equation formulation with electromagnetic reciprocity invoked to construct the inverse relationship. The functional relating the data and the conductivity distribution is non-linear, therefore a linearized inverse solution must be improved iteratively until an appropriate stopping criterion is satisfied. The unstable nature the inversion requires regularization and we use the Marquardt damping technique (Marquardt, 1963). The inversion solution is in the frequency-domain and time-domain field data are transformed to the frequency-domain via application of an FFT (Eaton and Hohmann, 1987). The program is designed so that user input parameters such as the horizontal and vertical zone of investigation, the regularization technique, and the survey configuration are variable. In this way the routine can be adjusted for use with a variety of EM methods, and rigorous Backus-Gilbert (1968) appraisal can be applied.

Formulation of the Frechet kernel

The perturbation of a 3-D conductivity structure, $\delta\sigma$, gives rise to a perturbation of the electric field, E, and the magnetic field, H. The relationship between the magnetic field,

the conductivity perturbation and the total electric field is given by the integral equation,

$$\mathbf{H}^+ = \mathbf{H} + \int_V \bar{\mathbf{G}}^H \mathbf{E}^+ \delta\sigma dV,$$

where the plus superscript indicates the total field vector after the perturbation of σ , \mathbf{E}^+ is the total electric field in the 3-D volume V, and the tensor $\bar{\mathbf{G}}^H$ is the 3-D magnetic field Green's function for the unperturbed model. Rewriting this equation yields a Fredholm integral equation of the first kind, where changes in the response, $\delta\mathbf{H}$ are related to changes in model parameters, $\delta\sigma$, by

$$\mathbf{H}^+ - \mathbf{H} = \delta\mathbf{H} = \int_V \bar{\mathbf{G}}^H (\mathbf{E} + \delta\mathbf{E}) \delta\sigma dV.$$

By ignoring the smaller, second order term, $\delta\mathbf{E}\delta\sigma$, we obtain the Born approximation, and have

$$\delta\mathbf{H}(\mathbf{r}_0) = \int_{V'} \bar{\mathbf{G}}^H(\mathbf{r}_0, \mathbf{r}') \mathbf{E}(\mathbf{r}') \delta\sigma(\mathbf{r}') dV' \quad (1)$$

where the spatial positions are now given explicitly: \mathbf{r}_0 denotes the receiver coordinates and \mathbf{r}' the anomalous conductivity source coordinates.

Using only the vertical component of the magnetic field in the inversion equation (1) reduces to

$$\begin{aligned} \delta H_z(\mathbf{r}_0) = \int_{V'} & \left((G_{zx}^H(\mathbf{r}_0, \mathbf{r}') E_x(\mathbf{r}') + \right. \\ & \left. (G_{zy}^H(\mathbf{r}_0, \mathbf{r}') E_y(\mathbf{r}') + \right. \\ & \left. (G_{zz}^H(\mathbf{r}_0, \mathbf{r}') E_z(\mathbf{r}') \right) \delta\sigma(\mathbf{r}') dV'. \end{aligned}$$

The 3-D dyadic Green's function, $\bar{\mathbf{G}}^H$, is essentially the magnetic field at the receiver, \mathbf{r}_0 , due to a unit electric dipole source at \mathbf{r}' . Applying EM reciprocity, this is equivalent to an electric field at \mathbf{r}' due to a magnetic current dipole source at the receiver position, \mathbf{r}_0 . Therefore $G_{zx}^H(\mathbf{r}_0, \mathbf{r}')$, a z-directed magnetic field due to an x-directed unit electric dipole source, can be expressed as a function of $E_{xz}^H(\mathbf{r}', \mathbf{r}_0)$, an x-directed electric field due to a z-directed magnetic current dipole source. Replacing the magnetic Green's function with the reciprocal electric field yields

$$\begin{aligned} \delta H_z(\mathbf{r}_0) = \frac{-1}{i\omega\mu_0} \int_{V'} & \left((E_{xz}^H(\mathbf{r}', \mathbf{r}_0) E_x(\mathbf{r}') + \right. \\ & \left. (E_{yz}^H(\mathbf{r}', \mathbf{r}_0) E_y(\mathbf{r}') + \right. \\ & \left. (E_{zz}^H(\mathbf{r}', \mathbf{r}_0) E_z(\mathbf{r}') \right) \delta\sigma(\mathbf{r}') dV'. \quad (2) \end{aligned}$$

The reciprocal electric field is due to a source with unit moment located at the center of the loop, while the original electric field is due to the transmitter.

Discretization of the volume, V , depends on the inherent resolution of a particular EM method. For the central-loop configuration, the volume is discretized into columns of blocks with the sides defined by the transmitter loop, as shown in Figure 1. The horizontal extent of the columns reflects the limits to which we can resolve the earth with central-loop geometry. The vertical dimension of each cell is also fixed and reflects the decrease in resolution with increasing depth. The center of the shallowest cell is at a depth of one half the skin depth for the highest frequency in the sounding. Each of the four shallowest cells have a thickness of one quarter the length of the side of the transmitter loop. The thickness of the next four cells is one half the length of the side of the transmitter loop in depth extent and the vertical extent of the last two cells are equal to the length of the transmitters side. The algorithm allows for discretization of the earth to a depth equal to five transmitter side lengths. It is important to consider the depth to which the inversion will operate.

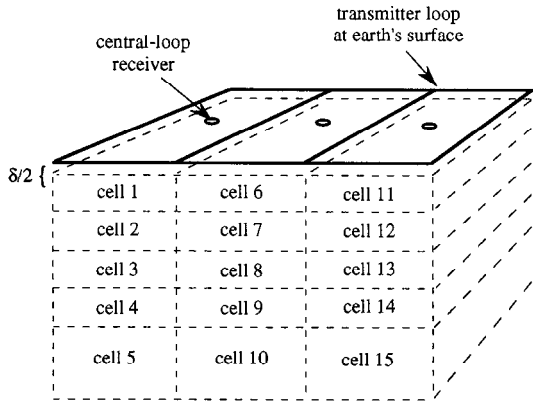


Figure 1. Inversion geometry for a grouping of three central-loop EM soundings and five vertical cells per sounding. The depth to the first layer of cell centers is one-half the skin depth of the highest frequency in the host medium.

Within a particular cell, the electric field and conductivity are constant and the integral of equation (2) is replaced with a summation over the M cells. The magnetic and electric field strengths are measured or are transformed to NFREQ distinct frequencies and the total number of data points N is $NFREQ * NS$, where NS is the number of soundings in a inversion grouping. Dropping the explicit reference to the receiver, \mathbf{r}_o , indexing \mathbf{r}' with j , and indexing the data points with i , equation (2) becomes

$$\delta H_i = \sum_{j=1}^M D_{i,j} \delta \sigma_j \quad (3)$$

where

$$D_{i,j} = \frac{-vol_j}{i\omega_j \mu} (\mathbf{E}_{i,j}^R \cdot \mathbf{E}_{i,j}^S)$$

is the Frchet kernel that relates changes in the model parameter, $\delta \sigma$, to changes in the response, δH . The superscripts R and S denote the electric field due to the reciprocal source and the survey transmitter and vol_j is the volume of the j th cell.

The Inverse Solution

The change in the magnetic field from the k to $k+1$ iteration is given by

$$H_i^{k+1} - H_i^k = \sum_{j=1}^M D_{i,j}^k \delta \sigma_j^k$$

and the residual or error, e_i , relative to the observed data, H_i^d , at the k^{th} iteration is

$$e_i^k = H_i^d - H_i^k,$$

so that

$$e_i^k - e_i^{k+1} = \sum_{j=1}^M D_{i,j}^k \delta \sigma_j^k \quad (4)$$

The least-squares minimization of the residual or error in equation (4) is numerically unstable and requires some form of regularization. Although many regularization techniques can be implemented, for this test we use a least-squares minimization of the error subject to the minimization of the solution length, which leads to the Marquardt solution (1963)

$$\delta \mathbf{m} = [\bar{\mathbf{D}}^T \bar{\mathbf{D}} + \lambda^2 \bar{\mathbf{I}}]^{-1} \bar{\mathbf{D}}^T \mathbf{e}^k,$$

where λ^2 is the Lagrange multiplier or the Marquardt parameter. λ serves to numerically stabilize the $\bar{\mathbf{D}}^T \bar{\mathbf{D}}$ matrix. We use

$$\lambda^2 = \alpha \left(\sum_{i=1}^N \sum_{j=1}^M \gamma_{i,j} \gamma_{i,j}^* \right)^{1/2}$$

where $\gamma_{i,j}^*$ is the complex conjugate of an element $\gamma_{i,j}$ of the $\bar{\mathbf{D}}^T \bar{\mathbf{D}}$ matrix and α is chosen in accordance with the change in error at each iteration (Oristaglio and Worthington, 1980), so that the solution moves between the steepest descent and the Gauss-Newton solution.

The iterative inverse solution starts with an initial estimate of the anomalous conductivity, such as a half space estimate or a 1-D interpretation. At the k th iteration we have

$$\sigma^k = \sigma^{k-1} + \delta \sigma^{k-1}$$

The anomalous conductivity, σ^k , is used to compute new electric and magnetic fields at the k^{th} iteration, which in turn are used to update the Frchet kernel and the residual. An iteration cycle is complete when a new conductivity estimate is calculated from the new kernel and residual. Finding an appropriate stopping criteria proved to be difficult for inversion of a perfect model, because the discretization used to compute the synthetic data is exactly that used in the inverse algorithm, and the final fit can be within machine precision. Such precision is not appropriate for the inversion of real measurements. Experimentation shows that the error between the inverse solution and the true model is within 10 percent for seven to nine iterations for a wide variety of starting models. When the solution is within 10 percent of its true value, the error is within 10 percent of the values of the secondary field; a reasonable stopping criteria for field data.

When data with 2-D surface coverage is available, four to eight columns of cells surrounding a given receiver can be simultaneously inverted. For profile data an iteration is performed for groups of four to five soundings along the profile line, moving across the profile one sounding at a time. One iteration is performed on the cells beneath the terminal soundings at each end of the profile, two iterations are performed on the cells beneath the soundings located one loop in from the end and so forth toward the center of the profile. The estimated resistivity values in each cell are then arithmetically averaged to construct a final model. Resistivity values for cells at the ends of the profile lines are averaged with the value of the host to stabilize poorly resolved end cells and to provide a smooth transition from the discretized survey area to the host background. It is therefore important to have a reliable estimate of the background resistivity in the survey area.

Inversion performance

To demonstrate the performance of the algorithm, we inverted the response of two models: a simple prism and a simulated contaminant plume. The forward response of the simple prism model is computed with the same discretization used in the inversion algorithm and serves to demonstrate the strengths and weaknesses of the algorithm without undue complication. The synthetic data for the plume is computed with a discretization much finer than that used in the inverse parameterization in an effort to simulate field data. Inasmuch as a refinement of a 1-D interpretation is the object of this scheme, we compare a 1-D interpretation to the 3-D interpretations. A current filament image inversion is used instead of a traditional layered-earth formulation because it is more robust in the presence of 3-D structures (Eaton and Hohmann, 1989).

Figure 2 shows the geometry for a simple four celled prism. The model illustrates how well the inversion works under ideal circumstances, and serves as a benchmark for further refinement of the algorithm. Using four soundings per grouping, an inversion depth of four cells, and starting models of a 130 ohm-m half space and the 1-D image model, the 3-D inversion yields the values shown in Figure 3c and 3d, respectively. Compared to the 1-D image solution in Figure 3b, both 3-D solutions are excellent. Resistivity distortions on the order of 5 percent are present for both starting models, while the 1-D solution displays distortions in excess of 25 percent.

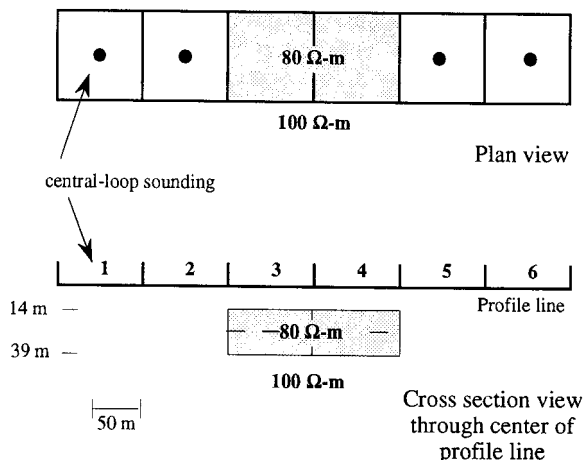


Figure 2. Geometry of a simple test model - a prism embedded in a half-space.

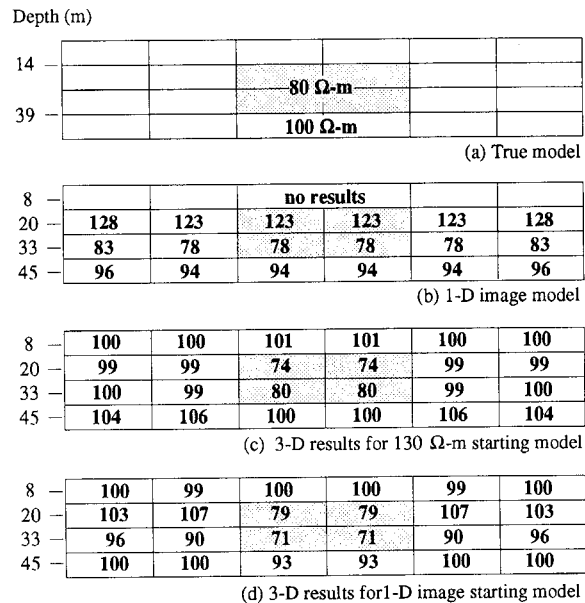


Figure 3. Inversion results for the prism model of figure 2 along the profile line. The inversion ran for seven iterations using four vertical cells per sounding, and four soundings per grouping. Cells resistivity values in ohm-m.

An examination of the Fréchet kernel provides a measure of the relative influence of the various cells. We find that very little information is obtained from the zone more distant than two transmitter lengths from the receiver. Increasing the number of soundings per grouping increases computer run times and degrades the solution. An increase from four soundings per grouping to five increased the run time by a factor of three. The line is only six soundings long and if five are used in each grouping, the line allows just two groupings. This means the final value of the interior cells is the average of only two inversion estimates instead of the three obtained when four soundings per partition are used. If the profile were longer we expect that the results would not be as sensitive to the size of the grouping.

The geometry of the plume model is illustrated in Figure 4. This model serves to investigate the problem of mapping a conductive contaminant plume. The model simulates a 5 ohm-m plume injected at a point and confined to a horizontal layer. The uniform 25 ohm-m host resistivity is taken to be that of the groundwater that saturates an unconsolidated sandy fluvial system. The variables set in the 3-D inversion include four soundings per grouping, a depth of exploration of 1.5 transmitter loop side lengths, and two starting models - a 30 ohm-m half-space, and the 1-D image estimate. The stopping criteria was achieved in five iterations.

Figure 5 shows the true model, 1-D image estimate and 3-D results for two starting models along the profile line. The inversion scheme does quite well in defining the base of the plume yet overestimates the plume resistivity. Use of a half-space starting model yields a model in which the host is quite well resolved, while the target resistivity is overestimated. The 1-D image solution yields results in which the resistivity of the plume is better resolved than with the half-space starting model, but the host is better resolved in the half-space model. The estimated model resulting from the half-space starting model shifts the plume vertically upward, but does resolve its base. This is an unexpected and currently unexplained feature of the inversion. In contrast, the 1-D image starting model solution

yields an estimated model in which the plume is well located vertically, while the base is poorly resolved. Both solutions show notable improvement over the 1-D interpretation.

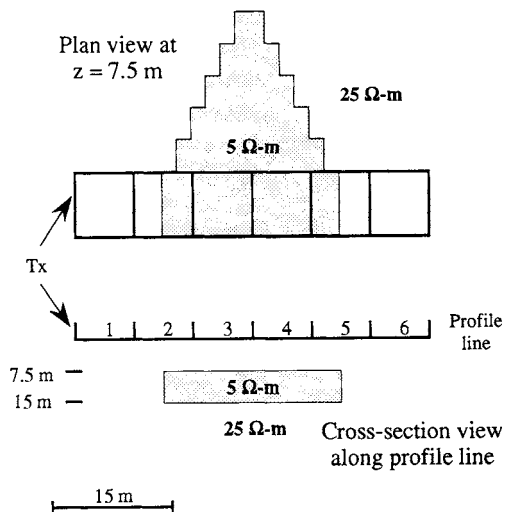


Figure 4. Geometry for the contaminant plume model at the top of the plume, $z = 7.5$ m. Transmitters are 7.5 m on a side. There are six transmitters along the profile line.

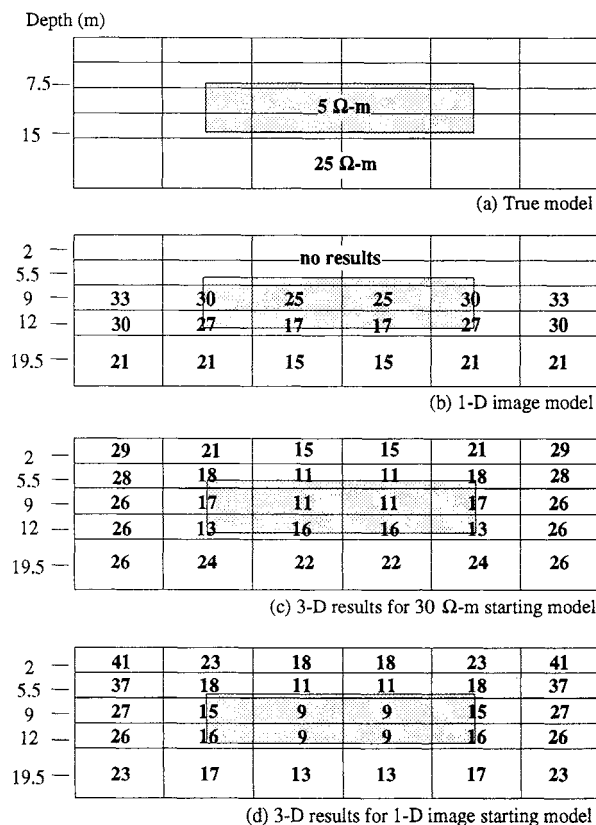


Figure 5. Inversion results for the plume model of figure 4 along the profile line. The inversion ran for five iterations using five vertical cells per sounding, and four soundings per grouping. Cells resistivity values in ohm-m.

Conclusions

One-dimensional inversion techniques have become standard tools for the interpretation of EM data. While they are not always structurally appropriate, a 1-D interpretation can be valuable as a starting point for extending interpretation to higher dimension. We account for the lateral effects that distort a 1-D response by using a 3-D algorithm that has the flexibility of varying many important variables to generate a suite of models, thereby limiting numerical artifacts in the interpreted model. The availability of fast, small computers has made 3-D inversion practical. Run times on a Sparc workstation vary between 1 to 4 hours for the examples presented. Thus data collected in a day can be interpreted overnight.

With most model-fitting type inversion techniques, the starting model affects the final solution. In example 1, the simple prism, the 1-D interpretation is strongly distorted and the half-space starting model yields the best result. When the 1-D interpretation is used as a starting model some of the distortions are retained in the 3-D inversion. Both starting models used in the inversion of the contaminant plume of example 2 yield reasonable estimates, although each starting model yields different characteristics in terms of the spatial location of the plume. To properly use a model-fitting inversion scheme the inversion variables - especially the starting models - should be varied and the algorithm rerun to generate a suite of models. Essential features in the models can then be recognized using the rigorous appraisal techniques of Backus and Gilbert (1968) to form a final geoelectric model.

Acknowledgments

The authors would like to thank the members of the Consortium of Electromagnetic Modeling and Inversion (CEMI) at the University of Utah for their financial and technical support, and the electromagnetic modeling group for many stimulating discussions. The San Diego Supercomputer Center Cray Y-MP8/864 supplied much of the computing time.

References

- Blohm, M., Hoekstra, P., Blohm, R., 1991, Utility and limitations of 1-D inversions of time-domain EM data over strong 2D structures: SEG 61st Annual International Meeting and Exposition, Expanded Abstracts, 410-411.
- Backus, G.E., and Gilbert, J.F., 1968, The resolving power of gross earth data: *Geophys. J. R. Astr. Soc.*, 16, 169-205.
- Eaton, P.A., and Hohmann, G.W., 1987, An evaluation of electromagnetic methods in the presence of geologic noise: *Geophysics*, 52, 1106-1126.
- Eaton, P.A., and Hohmann, G.W., 1989, A rapid inversion technique for transient electromagnetic soundings: *Physics of the Earth and Planetary Interiors*, 53, 394-404.
- Eaton, P.A., 1989, 3D electromagnetic inversion using integral equations: *Geophys. Prosp.*, 37, 407-426.
- Marquardt, D.W., 1963, An algorithm for least-squares estimation of non-linear parameters: *J. SIAM*, 11, 431-441.
- Newman, G.A., Anderson, W.L., and Hohmann, G.W., 1987, Interpretation of electromagnetic soundings over three-dimensional structures for the central-loop configuration: *Geophys. J. R. Astr. Soc.*, v. 89, 889.
- Oristaglio, M.L., and Worthington, M.H., 1980, Inversion of surface and borehole electromagnetic data for two-dimensional electrical conductivity models: *Geophysical Prospecting*, 28, 633-657.
- Taylor, K., Widmer, M., and Chesley, M., 1992, Use of transient electromagnetics to define local hydrogeology in an arid alluvial environment: *Geophysics*, 57, 343-352.